INTERNATIONAL JOURNAL FOR NUMERICAL METHODS IN FLUIDS, VOL. 20, 341–361 (1995)

A COMPOSITE MULTIGRID METHOD FOR CALCULATING UNSTEADY INCOMPRESSIBLE FLOWS IN GEOMETRICALLY COMPLEX DOMAINS

Y. ZANG AND R. L. STREET

Environmental Fluid Mechanics Laboratory, Stanford University, Stanford, CA 94305-4020, U.S.A.

SUMMARY

A time-accurate, finite volume method for solving the three-dimensional, incompressible Navier–Stokes equations on a composite grid with arbitrary subgrid overlapping is presented. The governing equations are written in a non-orthogonal curvilinear co-ordinate system and are discretized on a non-staggered grid. A semi-implicit, fractional step method with approximate factorization is employed for time advancement. Multigrid combined with intergrid iteration is used to solve the pressure Poisson equation. Inter-grid communication is facilitated by an iterative boundary velocity scheme which ensures that the governing equations are well-posed on each subdomain. Mass conservation on each subdomain is preserved by using a mass imbalance correction scheme which is second-order-accurate. Three test cases are used to demonstrate the method's consistency, accuracy and efficiency.

KEY WORDS Navier–Stokes; unsteady; composite multigrid; incompressible; non-staggered grid; semi-implicit

1. INTRODUCTION

The domain of most engineering and environmental flows is highly complex and irregular. One of the powerful tools to tackle complex geometry is the use of a non-orthogonal body-fitted curvilinear grid. However, it is often difficult or inefficient to cover an irregular domain with a single grid and it is therefore necessary to use domain decomposition and composite grids. Moreover, with the increasing importance of parallel or distributed computation, the domain decompostion method proves a great advantage in achieving high computing performance.

Figure 1 shows a composite grid which consists of three overlapping subgrids G_1, G_2 and G_3. Two kinds of boundaries exist in the subgrids, namely the 'physical boundary' which encloses the physical domain and the 'inter-grid boundary' which lies in the interior of neighbouring subgrids. For example, in subgrid G_2 (Figure 1) AB and CD are physical boundaries and BC and DA are inter-grid boundaries. The region enclosed by AFED is called the 'overlapping zone' between subgrids G_1 and G_2.

Extensive work has been done on composite grid methods for solving compressible flows; see e.g. References 1 and 2 in which both overlapping and patching or touching subgrids have been used. The development of this technique in treating incompressible flows is more recent. In solving incompressible flows, overlapping subgrids are usually employed. Meakin and Street[3] investigated the domain decomposition method and simulated flows in a model lake. They solved the incompressible Navier–Stokes equations implicitly and used Schwarz iteration to achieve global

CCC 0271–2091/95/050341–21

Received 9 October 1992
Revised 30 July 1994

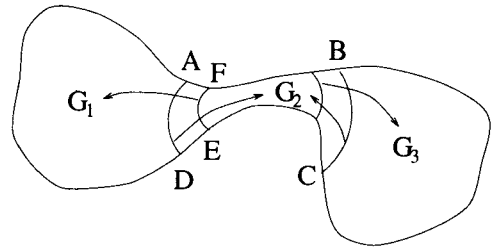

Figure 1. A composite grid consiting of three overlapping subgrids

convergence. Van der Wijngaart[4] developed a general data structure for two-dimensional composite grids and used the modified staggered grid to solve steady flow problems. Stüben and Trottenberg[5] and Henshaw ans Chesshire[6] discussed composite multigrid methods for solving model PDEs. Hinatsu and Ferziger[7] explored the efficiency of different composite multigrid schemes using 1D and 2D model problems. Tu and Fuchs[8] investigated overlapping grids and multigrid methods in calculations of unsteady flows in IC engines. Berger and Oliger,[9] Caruso *et al.*[10] and McCormick and Thomas[11] developed multidomain methods for adaptive grid applications. Perng and Street[12] recently introduced a new method to obtain multiple-domain solutions for incompressible flows which updates the velocity field independently on each subgrid and solves the pressure field globally by sweeping through the subgrids. This procedure reduces the cost of computation significantly compared with conventional methods which iterate both the momentum and pressure equations through subdomains.[3] Their computations of flows in complex cavities and ducts showed good global consistency and accuracy. However, Perng and Street required that the grid points from different subgrids in the overlapping zone be coincident, which is difficult to realize when constructing a composite grid over irregular domains.

Before presenting the objectives of the present work, we first give the definitions of several key terms which are to be used throughout this paper. We define that the solution on a composite grid is consistent if the difference between physical quantities obtained from overlapping subgrids at a fixed spatial point is of the same order as that of the overall solution method which includes discretization, solution and interpolation. In other words, if q_1 and q_1 are the calculated values of a physical quantity q on subgrids G_1 and G_2, respectively, the solution on the composite grid consisting of G_1 and G_2 is consistent if the following is true for all q:

$$|q_1(x_i, t) - q_2(x_i, t)| < \varepsilon \sim O(1/N^m), \tag{1}$$

where N is the number of grid points in one spatial dimension and m is the order of accuracy of the overall solution method.

Since the fluid is of constant density and incompressible, the mass is conserved on a subgrid G_i if

$$\int_{\partial G_i} u_j n_j \, dS = 0, \tag{2}$$

where ∂G_i represents the boundary of G_i, u_j is the velocity and n_j is the outward unit normal of ∂G_i.

We say that an interpolation scheme is conservative if

$$\int_{\partial G_i^P} u_j n_j \, \mathrm{d}S + \int_{\partial G_i^I} u_j^I n_j \, \mathrm{d}S = 0, \tag{3}$$

where ∂G_i^P and ∂G_i^I denote the physical and inter-grid boundaries of subgrid G_i, respectively and u_i^I is the velocity on the inter-grid boundary which is interpolated from neighbouring subgrids. The interpolation scheme is non-conservative if equation (3) is not satisfied.

In spite of the significant progress which has been achieved in solving incompressible flows on composite grids, important problems which have not been fully resolved still exist, such as those related to solution consistency, inter-grid boundary condition, mass conservation and coservative versus non-conservative interpolation. These problems lead to the following questions.

(a) How can solution consistency be achieved on a general composite grid with arbitrary subgrid overlapping?
(b) What inter-grid boundary condition should be used?
(c) How should mass conservation on a subdomain be satisfied?
(d) What is the effect of mass imbalance due to the non-conservative interpolation scheme on the convergence of the composite multigrid method?

The present work is an attempt to address these questions. It extends the work of Perng and Street[12] to the case of general composite grids which do not require coincident grid points in the overlapping zone. Moreover, the solver is written in a non-orthogonal curvilinear co-ordinate system and is based on a non-staggered grid. Problems regarding the well-posedness of the governing equations on a general composite grid, the consistency of the global solution and the accuracy and efficiency of the composite multigrid method are discussed.

The governing equations are given in Section 2. In Section 3 we briefly describe the basic solution method. The composite grid procedure is detailed in Section 4. Results of three test cases are given in Section 5. Section 6 presents some concluding remarks.

2. GOVERNING EQUATIONS

The governing equations are the constant viscosity, constant density, three-dimensional, incompressible Navier–Stokes equations

$$\frac{\partial u_j}{\partial x_j} = 0 , \tag{4}$$

$$\frac{\partial u_i}{\partial t} + \frac{\partial}{\partial x_j}\left(u_j u_i\right) = -\frac{\partial p}{\partial x_i} + \nu \frac{\partial^2 u_i}{\partial x_j \partial x_j} , \tag{5}$$

where $i, j = 1, 2, 3$, u_i are the Cartesian velocity components, p is the pressure divided by the fluid density and ν is the kinematic viscosity. The above equations are transformed into the general curvilinear co-ordinate system in strong conservation law form[13] as

$$\frac{\partial U_m}{\partial \xi_m} = 0 , \tag{6}$$

$$\frac{\partial (J^{-1} u_i)}{\partial t} + \frac{\partial F_{im}}{\partial \xi_m} = 0 , \tag{7}$$

where $m = 1, 2, 3$, the flux is

$$F_{im} = U_m u_i + J^{-1} \frac{\partial \xi_m}{\partial x_i} p - \nu J^{-1} g^{mn} \frac{\partial u_i}{\partial \xi_n} , \tag{8}$$

U_m is the volume flux (the contravariant velocity multiplied by the inverse of the Jacobian or the volume of the computational cell) normal to a surface of constant ξ_m, J^{-1} is the inverse of the Jacobian

or the volume of the cell and g^{mn} is the contravariant metric tensor. Accordingly,

$$U_m = J^{-1} \frac{\partial \xi_m}{\partial x_j} u_j , \tag{9}$$

$$J^{-1} = \det\left(\frac{\partial x_i}{\partial \xi_j}\right) , \tag{10}$$

$$g^{mn} = \frac{\partial \xi_m}{\partial x_j} \frac{\partial \xi_n}{\partial x_j} . \tag{11}$$

3. BASIC NUMERICAL METHOD

In this section we briefly describe the basic solution method on a single grid. The details are presented in Reference 14. The governing equations are discretized using the finite volume method on a non-staggered grid. The pressure and the Cartesian velocity components u_i are defined at the centre of the control volume, while the volume fluxes U_m are defined on the corresponding faces (see Figure 2). The Adams–Bashforth/Crank–Nicolson scheme[15] is used to advance the governing equations semi-implicitly in time. The discretized equations are

$$\frac{\delta U_m}{\delta \xi_m} = 0 , \tag{12}$$

$$J^{-1} \frac{u_i^{n+1} - u_i^n}{\Delta t} = \tfrac{3}{2}\left[C_i^n + D_E(u_i^n)\right] - \tfrac{1}{2}\left[C_i^{n-1} + D_E(u_i^{n-1})\right] + R_i(p^{n+1}) + \tfrac{1}{2}\left[D_I(u_i^{n+1} + u_i^n)\right] , \tag{13}$$

where $\delta/\delta\xi_m$ denotes the discrete finite difference operator in computational space, superscripts represent the time step, C_i is the convective term, R_i is the discrete operator for the pressure gradient terms and D_E and D_I are discrete operators representing the explicitly treated off-diagonal viscous terms and the implicitly treated diagonal viscous terms respectively.

All the spatial derivatives are approximated with second-order central differences, with the exception of the convective terms which are discretized using a variation of QUICK.[16]

Application of the fractional step method to (13) leads to the following predictor–corrector solution procedure.

1. Predictor:

$$\left(I - \frac{\Delta t}{2J^{-1}} D_I\right)(u_i^* - u_i^n) = \frac{\Delta t}{J^{-1}} \left\{\tfrac{3}{2}\left[C_i^n + D_E(u_i^n)\right] - \tfrac{1}{2}\left[C_i^{n-1} + D_E(u_i^{n-1})\right] + D_I(u_i^n)\right\} . \tag{14}$$

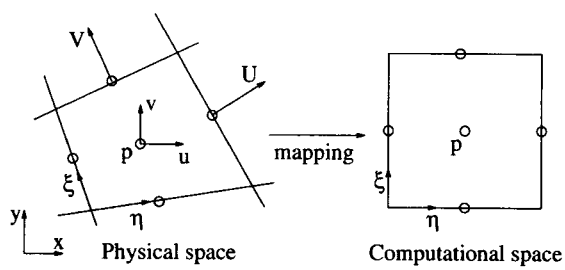

Figure 2. A control volume of the non-staggered grid and the co-ordinate mapping in two dimensions

2. Corrector:

$$u_i^{n+1} - u_i^* = \frac{\Delta t}{J^{-1}} \left[R_i(\phi^{n+1})\right] . \tag{15}$$

Where I is the identity matrix and u_i^* is called the intermediate velocity. The variable ϕ is related to the pressure p by

$$R_i(p) = \left(J^{-1} - \frac{\Delta t}{2} D_I\right) \frac{R_i(\phi)}{J^{-1}} ; \tag{16}$$

hereafter ϕ is referred to as the 'pressure'.

Equation (14) is solved with the approximate factorization technique[17,18] in which the left-hand side (LHS) of (14) is factorized into three tridiagonal matrices as

$$\left(I - \frac{\Delta t}{2J^{-1}} D_1\right)\left(I - \frac{\Delta t}{2J^{-1}} D_2\right)\left(I - \frac{\Delta t}{2J^{-1}} D_3\right)(u_i^* - u_i^n) = \text{RHS of (14)} , \tag{17}$$

where $D_k (k = 1, 2, 3)$ is the discrete one-dimensional diagonal viscous operator and $D_I = D_1 + D_2 + D_3$. After the corrector step (15) the volume flux is updated with

$$U_m^{n+1} = U_m^* - \Delta t\left(J^{-1} g^{mn} \frac{\delta \phi^{n+1}}{\delta \xi_n}\right) , \tag{18}$$

where $U_m^* = J^{-1}(\delta \xi_m / \delta x_j) u_j^*$ which is defined on the cell faces is called the intermediate volume flux. To calculate U_m^*, the value of u_i^* which is defined at the cell centre is first interpolated onto the cell faces with a third-order quadratic upwind interpolation scheme similar to that used in QUICK. After u_i^* is obtained on the cell face, U_m^* is calculated according to its definition above.

Before u_i^{n+1} can be obtained from (15) or U_m^{n+1} from (18), we need to solve for ϕ^{n+1} from the following pressure Poisson equation, which is derived by substituting equation (18) into the continuity equation (12):

$$\frac{\delta}{\delta \xi_m}\left(J^{-1} g^{mn} \frac{\delta \phi^{n+1}}{\delta \xi_n}\right) = \frac{1}{\Delta t} \frac{\delta U_m^*}{\delta \xi_m} . \tag{19}$$

The above equation is valid for interior cells. For the cells adjacent to a physical boundary the volume flux U_m on the boundary is known from the boundary condition (zero on a solid wall). Therefore this term in equation (12) is not replaced by (18); instead, the prescribed boundary condition is used. For example, for the control volume adjacent to the $\xi = 0$ boundary (Figure 3) the form of the pressure Poisson equation is (in two dimensions)

$$U_{5/2,j}^* - U_{3/2,j}^{n+1} + V_{2,j+1/2}^* - V_{2,j-1/2}^* = \Delta t \left[\left(J^{-1} g^{1n} \frac{\partial \phi}{\partial \xi_n}\right)_{5/2,j} + \left(J^{-1} g^{2n} \frac{\partial \phi}{\partial \xi_n}\right)_{2,j-1/2}\right] - \left(J^{-1} g^{2n} \frac{\partial \phi}{\partial \xi_n}\right)_{2,j-1/2} . \tag{20}$$

On a physical boundary the second term on the LHS of (20), $U_{3/2,j}^{n+1}$, is obtained from the prescribed boundary condition. We note that there are no gradient terms of ϕ on and normal to the boundary on the RHS of the above equation.

For a non-orthogonal grid the value of ϕ outside the boundary may need to be computed. For example, when $V_{2,j+1/2}^{n+1}$ is calculated from equation (18), ϕs at the fictitious points i=1 are needed if central differencing is employed. In this work they are calculated as follows. We first obtain the

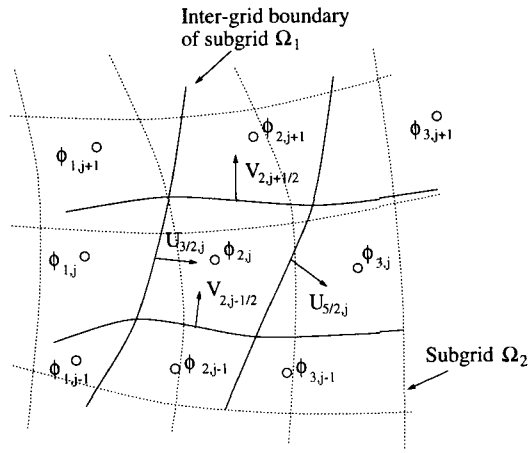

Figure 3. Sketch of the grid near an inter-grid boundary

gradient of ϕ on a given boundary by applying the normal momentum equation (18) on that boundary. The value of U_m^* in (18) is extrapolated from the interior. The value of ϕ outside the boundary can then be calculated from the normal gradient. It has been shown[19] that using the normal momentum equation provides the appropriate boundary condition for the pressure.

If the boundary at $i = \frac{3}{2}$ is an inter-grid boundary, then $U_{3/2,j}^{n+1}$ is unknown *a priori*. In this case $U_{3/2,j}^{n+1}$ is obtained in the iterative process in which ϕ^{n+1} is calculated. This is discussed in Section 4.1.

4. COMPOSITE GRID METHOD

To solve the governing equations on a composite grid, we employ a scheme similar to that of Perng and Street.[12] Their explicit scheme differs from conventional composite grid methods in that it involves inter-grid iteration only at the stage where the pressure Poisson equation is solved. In the present semi-implicit method, in addition to the above process for the pressure, iterations may also be needed when the factorized matrix is solved in the predictor step (17), since u_i^* is unknown on inter-grid boundaries. The basic steps of the composite grid method are as follows.

(a) *Predictor*: obtain u_i^* by solving (17); interpolate u_i^* onto the cell faces and compute U_m^*.
(b) *Pressure:* iterate (19) through all the subgrids to obtain a globally converged field of ϕ^{n+1}.
(c) *Corrector:* update the velocity u_i^{n+1} from (15) and the volume flux U_m^{n+1} from (18) on each subgrid independently.

When the above solution procedure is applied to an artibrarily overlapping composite grid, several issues arise. First, the solutions from different subgrids must be consistent with each other according to the definition given in Section 1 (equation (1)). Inconsistency may occur if improper inter-grid boundary conditions are used. Second, mass conservation needs to be preserved on each subgrid (equation (2)). This is equivalent to the satisfaction of the compatibility condition for the pressure Poisson equation. Third, the efficiency of the composite multigrid method depends on the above two conditions. These issues are discussed in the following subsections.

4.1. Inter-grid boundary conditions

In order to obtain a consistent solution on an arbitrarily overlapping composite grid, data transfer on the inter-grid boundaries needs to be properly treated. In the present semi-implicit formulation two

types of inter-grid boundary conditions are required. One is the boundary value of u_i^* in the predictor step. On physical boundaries we calculate u_i^* using the method developed by LeVeque and Oliger,[20] which requires that

$$u_i^* = u_i^n - \frac{\Delta t}{J^{-1}} R_i(\phi^n) + O(\Delta t^2) . \tag{21}$$

On inter-grid boundaries the value of u_i^* may still be obtained from equation (21) or by a linear extrapolation in time. These schemes, while maintaining second-order accuracy and avoiding iterations, were found to give slight inconsistencies in u_i^{n+1}. To overcome this difficulty, we solve equation (17) iteratively through subgrids. The value of u_i^* on inter-grid boundaries is interpolated from neighbouring subgrids with u_i^* at the previous time step as its initial guess. Typically a couple of iterations are sufficient to produce a consistent u_i^{n+1}. This iteration is relatively inexpensive, because the right-hand side of (17) is fixed in the iteration and, in addition, the iteration is only needed in the direction where an inter-grid boundary exists.

The second type of inter-grid boundary condition is of the volume flux U_m^{n+1} when the pressure Poisson equation is solved on grid cells adjacent to an inter-grid boundary (equation (20)). As pointed out at the end of Section 3, on an inter-grid boundary U_m^{n+1} is not known *a priori*. The usual practice to obtain inter-grid boundary conditions for the pressure Poisson equation is to interpolate u_i^* or U_m^* from neighbouring subgrids to compute the source terms on the RHS of equation (19) while using some type of pressure boundary condition[7,12] for the pressure gradient terms on the left-hand side. Perng and Street[12] discussed the choices of pressure boundary conditions for the case of subgrids with coincident grid points. They suggested that either the pressure value or the normal pressure gradient may be used as the boundary condition. While this is true for the cases in their study, numerical tests carried out by the present authors showed that when subgrids had non-coincident grid points, the pressure gradient boundary condition still worked, while the use of the pressure value produced inconsistent solutions. The reason lies in the well-posedness of the governing equations and we see below that the pressure gradient boundary condition follows naturally from this view.

It is known that the incompressible Navier–Stokes equations are well-posed in a given domain if the velocity is prescribed on the boundary of that domain; no pressure boundary condition is required .[19] On a composite grid, in order to achieve solution consistency, it is vitally important that the governing equations be well-posed on each subdomain. This condition is satisfied if velocities on inter-grid boundaries of that subdomain can be determined (velocities on physical boundaries are known and imposed). To achieve this, we introduce the iterative boundary velocity scheme to iteratively update volume fluxes U_m^{n+1} in the process of solving for the pressure. Consider again the example given in Figure 3 and equation (20). If $i = \frac{3}{2}$ is an inter-grid boundary, then the second term on the LHS of (20), $U_{3/2,j}^{n+1}$, is unknown. However, since the point $(\frac{3}{2}, j)$ is in the interior of a neighbouring overlapping subgrid, $U_{3/2,j}^*$ and the pressure gradients at the same location can be interpolated from that subgrid. Then $U_{3/2,j}^{n+1}$ can be obtained by applying the normal momentum equation on the boundary $i = \frac{3}{2}$. In general, after the $(p-1)$th pressure iteration, U_m at the pth iteration, $U_m^{n+1,p}$, on the inter-grid boundary ξ_m is determined by

$$U_m^{n+1,p} = (U_m^*)_I - \Delta t \left[J^{-1} g^{mn} \left(\frac{\delta \phi^{n+1,p-1}}{\delta \xi_n} \right)_I \right], \tag{22}$$

where the subscript I denotes that the value is interpolated from neighbouring subgrids and the superscript $(n+1, p)$ denotes the pth pressure iteration at time step $n+1$. The value of $U_m^{n+1,p}$ is then used in the source term of equation (19) to calculate $\phi^{n+1,p}$.

When the pressure converges, $U_m^{n+1,p}$ converges to U_m^{n+1}. This ensures that the proper velocity

boundary condition is prescribed on all the boundaries of the given subdomain, physical as well as inter-grid ones. As a result the governing equation is well-posed on each subgrid.

We see from equation (22) that the present boundary velocity scheme produces the same effect as that of interpolating U_m^* and using the gradient as the boundary condition for pressure. The use of the pressure value as boundary condition is inconsistent with equation (22) and as a result produces inconsistent solutions.

4.2. Mass conservation

Conservation of mass is a very important property in the numerical computation of incompressible flows. The complication with a composite grid is that it is very difficult to construct a conservative interpolation scheme in a general non-orthogonal co-ordinate system. Meakin[21] employed a non-conservative interpolation scheme and utilized a mass imbalance correction (MIC) scheme to enforce mass conservation. In an MIC scheme the amount of mass residual on a given subgrid due to the non-conservative interpolation is subtracted out to exactly satisfy mass conservation. Meakin stated that the convergence rate was accelerated by 10% when the MIC was applied in every inter-grid iteration. However, Meakind did not evaluate the effect of his MIC scheme on the overall accuracy of the numerical method.

In the present work we use third-order Lagrangian biquadratic interpolation to transfer data between subgrids. This interpolation scheme is non-conservative; mass conservation in a subdomain based on the interpolated velocity on the inter-grid boundaries is not guaranteed if no correction is applied. As a result of the mass imbalance the compatibility condition of the pressure Poisson equation is not satisfied and thus its convergence is limited at some level which is determined by the interpolation error. During the iteration of solving for the pressure, as the residual mass approaches this limit, the rate of convergence may become very slow and the performance of the multigrid method deteriorates. To avoid this undesirable behaviour, we employ an MIC scheme to ensure that mass is exactly conserved in each subdomain so that the fast convergence of the multigrid is preserved.

In the present formulation the correction is made to the volume flux after it is computed from equation (22). The magnitude of the correction is proportional to the local volume flux according to the formula

$$\tilde{U}_m^{n+1,p} = U_m^{n+1,p} - \frac{\varepsilon_v |U_m^{n+1,p}|}{S} \frac{\mathbf{n} \cdot \mathbf{e}_m}{|\mathbf{n} \cdot \mathbf{e}_m|}, \tag{23}$$

where ε_v is the global mass imbalance and S is the sum of the absolute value of the volume fluxes over all inter-grid boundaries. They are defined as

$$\varepsilon_v = \sum_I \left(U_m^{n+1,p} \frac{\mathbf{n} \cdot \mathbf{e}_m}{|\mathbf{n} \cdot \mathbf{e}_m|} \right), \tag{24}$$

$$S = \sum_I |U_m^{n+1,p}|, \tag{25}$$

where Σ_I is the sum over all the inter-grid boundaries in a given subgrid, $\mathbf{e}_m$ is the unit vector in the direction of the co-ordinate line ξ_m and $\mathbf{n}$ is the outward normal unit vector of the inter-grid boundary surface.

According to Henshaw[22] and Oliger,[23] the order of accuracy of the interpolation scheme should be at least one higher than that of the discretization in order to preserve the overall accuracy of the solution scheme. Since our discretization is second order and the interpolation scheme is third-order, the above criterion is satisfied. In addition, it can be easily shown that the MIC scheme is second-order-accurate

(Appendix). Therefore the second-order accuracy of the overall solution method is preserved. This fact is also demonstrated by numerical tests in Section 5.

4.3. Multigrid on composite grid

Composite multigrid methods have been investigated extensively. Stüben and Trottenberg[5] and Henshaw and Chessire[6] solved model elliptic PDEs. Hinatsu and Ferziger[7] have carried out numerical experiments to test two kinds of composite multigrid method, namely, in their terminology, the complete composite multigrid (CCMG) method, which transfers data among subgrids at all multigrid levels, and the incomplete composite multigrid (ICMG) method, which only transfers data at the finest grid level. While Stüben and Trottenberg demonstrated a good convergence rate of a CCMC method, the results of Hinatsu and Ferziger with a 1D model equation and the 2D Poisson equation showed that CCMG did *not* converge faster than ICMG. Tu and Fuchs[8] used multigrid for both momentum and continuity equations and reported good convergence behaviour. Perng and Street[12] used an ICMG method in their domain decompostion procedure and showed a good convergence property.

We extended the composite multigrid method of Perng and Street[12] to general composite grids with arbitrary subgrid overlapping. The basic procedure is to apply the multigrid defect correction scheme (MG-CS) within each subgrid and sweep through subgrids globally until convergence is achieved. The present strategy is similar to the ICMG method of Hinatsu and Ferziger[7] in which data communication between subgrids only occurs at the finest grid level.

Our choice of an ICMG instead of a CCMG strategy was based on considerations of overall efficiency and robustness of the unsteady flow solver. In an ICMG method, because inter-grid data transfer only occurs at the finest grid level, it is straightforward to impose the boundary condition at coarser grid levels in a defect correction scheme, since the boundary condition is the same as in a single-grid case. On the other hand, if a CCMG method is employed in which data are transferred at all multigrid levels, it is difficult to implement the defect correction scheme on inter-grid boundaries. The reason is that at a coarser grid level the defect correction scheme calculates the error of the quantity on the grid one level finer. Since the error on a subgrid is not a physical quantity and depends on the numerical property of the particular subgrid, it is not likely to correlate with the error of a neighbouring subgrid of disparate property. Although an 'exact' scheme was outlined by Hinatsu and Ferziger[7] for computing the inter-grid boundary condition in a CCMG which can be used in a multidimensional problem with subgrids of disparate geometrical properties, it involves computing and storing quantities of all the finer grids at any given grid level and leads to a tedious procedure. Thus in a CCMG, instead of the defect correction scheme, the less efficient full approximate scheme (FAS) may have to be used.[24]

A more serious issue with the CCMG method is that the overlapping at the inter-grid boundary between two neighbouring subgrids diminishes when the mesh is continuously coarsened.[6] This makes a CCMG method less robust in a general composite grid consisting of overlapping curvilinear or irregular subgrids. Henshaw and Chesshire[6] utilized a sophisticated grid generation routine to produce coarser grids from the finer grid. They increased the area of overlapping when the grid is coarsened to maintain the number of grid points in the overlapping zone as a constant. Although they demonstrated favourable results using this scheme, the number of multigrid levels was limited by the amount of overlappping, since, as the grid continues to be coarsened, the area of overlapping at an inter-grid boundary may become so large that it extends itself outside the physical domain. Other remedies could be employed, such as retaining layers of finest grids near the inter-grid boundary, moving the inter-grid boundary at every multigrid level or using large overlapping regions. The effects of these special treatments on the accuracy and convergence of the solution method are generally negative and not fully assessed. With an ICMG method this problem of intergrid overlapping does not exist and the number of multigrid levels is only restricted by the number of grid points in the subgrid.

It is acknowledged that the CCMG method may be more effective in solving certain types of problems which require many iterations to converge. In the present unsteady flow solver, however, the convergence of the pressure Poisson equation at every time step typically requires only a few iterations. The use of an ICMG method appears to be more robust and cost-effective. A comprehensive comparison of the efficiency and applicability of the ICMG and CCMG in solving different types of flow problems, including both steady and unsteady situations, would be useful. Such an extensive effort, is unfortunately, beyond the scope of our present investigation.

We employ the V-cycle strategy in the multigrid within each subgrid. The adaptive W-cycle method[25] was also implemented and found to yield essentially the same convergence rate as the V-cycle, On each grid level within a subgrid the number of smoothing operations is fixed at typically two or three. We employ the four-colour line-by-line Gauss–Seidel (FC-LGS) scheme as the smoother.[26] This scheme is fully vectorizable and at the same time retains the good smoothing property of the original line-by-line Gauss–Seidel method. Both the restriction and interpolation operations are trilinear and are carried out in the computational space.

In the global sweep Meakin and Street[3] have shown that the more frequently the iteration is switched between subgrids, the faster is the overall convergence rate. Following this criterion, we perform only one V-cycle on each subgrid before switching to the next one. This ensures that information is transferred between subgrids as often as possible.

The present composite multigrid (CMG) procedure for the pressure Poisson equation is summarized as follows.

(a) At the pth iteration calculate $U_m^{n+1,p}$ on a given subgrid using equation (22).
(b) Correct $U_m^{n+1,p}$ using equation (23) to enforce mass conservation.
(c) Perform one multigrid V-cycle on this subgrid.
(d) Move to the next subgrid and perform steps (a)–(c) until all the subgrids are swept through.
(e) Repeat steps (a)–(d) until global convergence is achieved.

Global convergence of the pressure Poisson equation at each time step is achieved when the following are satisfied:

$$\varepsilon_p < \varepsilon_p^c \,, \tag{26}$$

$$\mathrm{d}\phi < \mathrm{d}\phi^c \,, \tag{27}$$

where ε_p is the averaged non-dimensional residual of the pressure Poisson equation and $\mathrm{d}\phi$ is the averaged relative change in the pressure values on the inter-grid boundaries; ε_p^c and $\mathrm{d}\phi^c$ are their corresponding threshold values, which are typically taken as 10^{-5}–10^{-6}.

The stability of the numerical method is restricted by the Courant condition. The Courant number is defined as

$$CFL = \left(\frac{|u_1|}{\Delta x} + \frac{|u_2|}{\Delta y} + \frac{|u_3|}{\Delta z}\right) \Delta t = \left(|U_{\xi_1}| + |U_{\xi_2}| + |U_{\xi_3}|\right) \frac{\Delta t}{J^{-1}} \,. \tag{28}$$

The stability condition of the present method requires that

$$CFL_{\max} < \bar{C} \sim O(1) \,, \tag{29}$$

where $CFL_{\max}$ is the maximum value obtained from (28) in the computational domain. Numerical experiments have shown that $\bar{C} < 1$ yields stable solutions. The present semi-implicit method removes the restrictive viscous stability limit. The inviscid Courant condition is not significant for unsteady flows, in which the time accuracy of the solution is required.

The computer code is fully vectorized. The typical CPU time per grid node per time step on a single processor of a Cray Y-MP is about 30 μs. The iterative solution of the pressure Poisson equation is the most CPU-intensive part of the solution procedure, consuming over 50% of the total CPU requirement at each time step.

5. RESULTS

We chose three test cases to evaluate the consistency, accuracy and efficiency of the present numerical method. The first has an analytical solution and is used to check the overall order of accuracy as a function of grid refinement. Then two and three subgrids are used in calculating two-dimensional flows in a lid-driven polar cavity. By use of this example, the issues regarding the efficiency of CMG in solving the pressure Poisson equation, the effect of the extent of grid overlapping and the order of accuracy of the MIC scheme are investigated. Finally, upwelling flow in a rotating container with a conical bottom is computed to demonstrate the efficacy of the method in treating non-orthogonal grid systems. We note that examples 1 and 3 with cylindrical geometry are solved routinely with the present composite grid technique, while with a polar co-ordinate system one has to invest heavily in special programming to account for the mathematical singularity at the co-ordinate origin.

5.1. Spin-down flow in a circular cylinder

We consider the time-dependent flow of a spin-down to rest. Initially the fluid is in solid body rotation with a two-dimensional circular cylinder at an angular velocity Ω. At time t_0 the cylinder is suddenly brought to rest. The fluid slows down as a result of the drag of the wall. The analytical solution of the azimuthal velocity is:[27]

$$\frac{u_\theta}{\Omega R} = -2\sum_{n=1}^{\infty} \frac{J_1(\lambda_n r/R)}{\lambda_n J_0(\lambda_n)} \exp\left(-\lambda_n^2 \frac{vt}{R^2}\right),$$

where λ_n denotes the nth root of the first-order Bessel function of the first kind, J_1, Ω is the initial angular velocity, R is the cylinder radius, v is the kinematic viscosity and t is time.

Figure 4 is a schematic diagram of the flow domain and the overlapping composite grid which consists of an outer annular grid with a periodic boundary and an inner rectangular grid. Figure 5 shows the azimuthal velocity as a function of radius and time. A uniform (34 × 34, 18 × 18) × 3 two-subgrid composite grid was used. The computed solution agrees well with the exact solution. In addition, the agreement of the solutions from two subgrids in the overlapping zone demonstrates the consistency of the present method. The maximum relative error scaled by the maximum velocity of the computed solution at the non-dimensional time tv/R^2 of 0·005 is plotted in Figure 6 as a function of mesh refinement. The *CFL* number was kept fixed. The slope of approximately − 2 demonstrates the

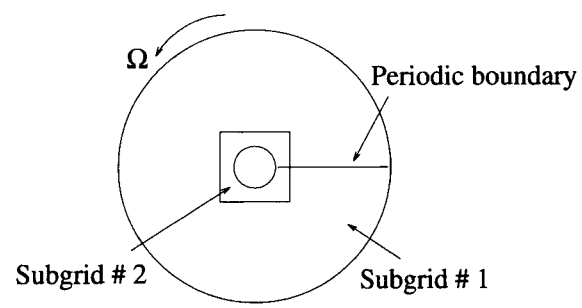

Figure 4. Domain and boundary condition for the spin-down flow to rest in a two-dimensional circular cylinder

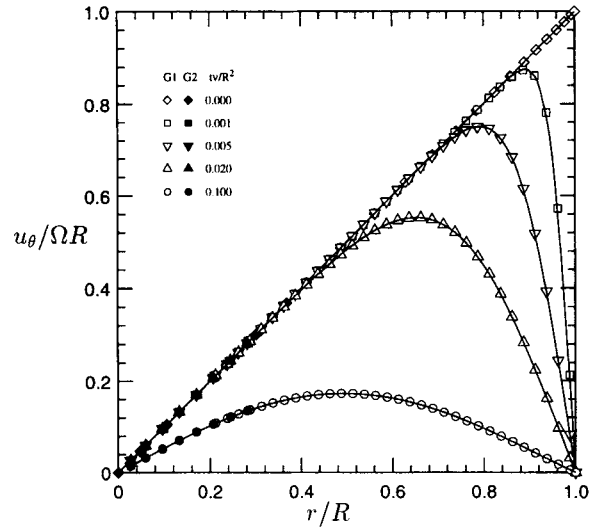

Figure 5. Azimuthal velocity profiles of the spin-down flow. Curves are from the analytical solution and symbols are from the present computation. G1, component grid 1; G2, component grid 2

fact that the overall accuracy of the method, including the discretization, the interpolation and the MIC scheme, is second-order in both space and time.

5.2. *Lid-driven polar cavity*

The two-dimensional flow in a lid-driven polar cavity at a Reynolds number of 350, based on the lid-velocity and the radius of the inner wall, was computed. The decomposed domain and the two-component composite grid are shown in Figure 7. The velocity profiles along the line of symmetry are plotted in Figure 8. The solution which was obtained on a non-uniform (34 × 50, 34 × 66) × 3 two-subgrid composite grid is compared with the experimental and numerical data of Fuchs and Tillmark[28]

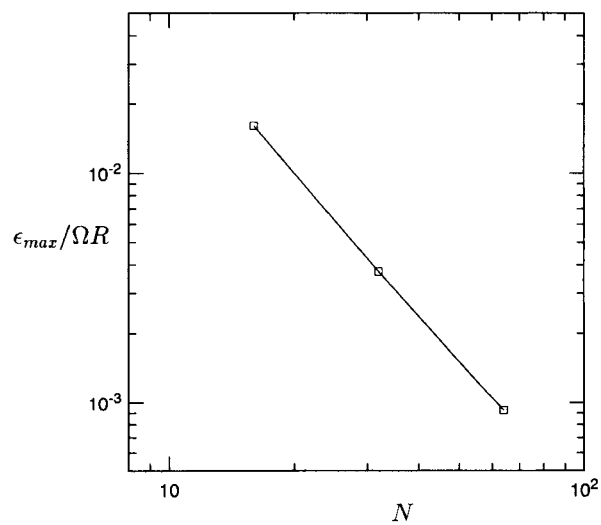

Figure 6. Maximum relative error of u_θ as a function of mesh refinement for the decaying vortices flow. N is the number of grid points in each dimension ($tv/R^2 = 0{\cdot}005$)

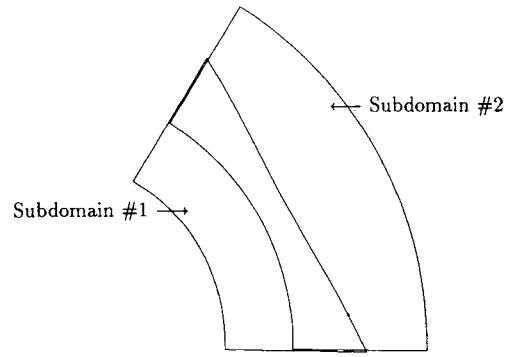

(a)

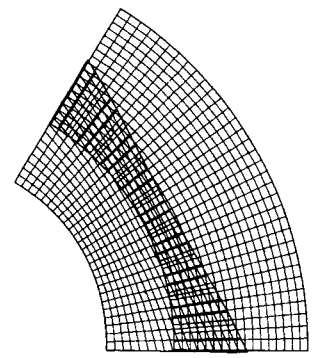

(b)

Figure 7. (a) Decomposed domain and (b) two-component composite grid for the flow in a lid-driven polar cavity

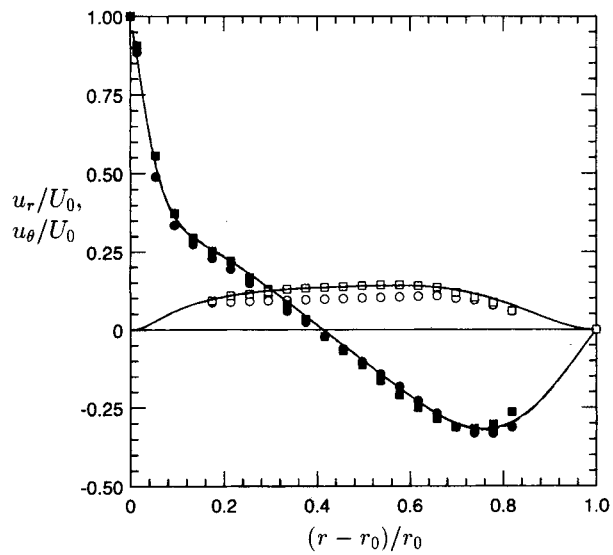

Figure 8. Comparison of the radial and azimuthal velocity profiles u_r and u_θ respectively along the radial line of symmetry (Re = 350). Symbols are from Reference 28: ●, u_θ, experiment; □, u_r experiment; ■, u_θ, computation; □, u_r, computation. Curves: – – –, present single grid; ——, present composite grid

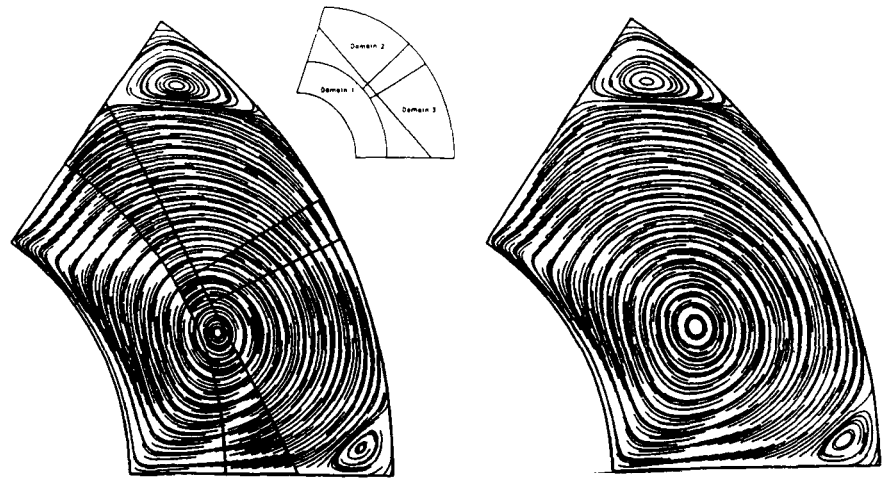

(a) (b)

Figure 9. Steady state streamlines of the lid-driven flow in a polar cavity: (a) composite grid solution; (b) single-grid solution

and also with a 66 × 66 × 3 single-grid solution employing the present method. The averaged relative error scaled with the lid velocity between the present composite grid and single-grid solutions is below 0·5%. Good agreement is also found between the present and Fuchs and Tillmark's numerical solutions. The discrepancy between the numerical and experimental data may be attributed to three-dimensional effects in the experiment.

In another case the polar cavity is decomposed into three subdomains (Figure 9(a)). The streamlines and vorticity contours at the steady state from the composite grid (Figures 9(a) and 10(a)) and single-grid (Figures 9(b) and 10(b)) solutions are compared. The composite grid solution accurately predicts the size and strength of both the primary and secondary eddies. The vorticity is shown because it is a

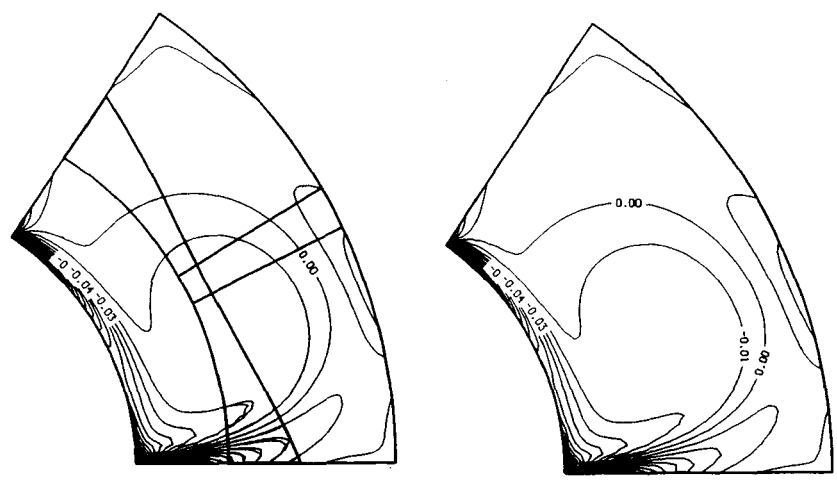

(a) (b)

Figure 10. Steady state vorticity contours of the lid-driven flow in a polar cavity: (a) composite grid solution; (b) single-grid solution

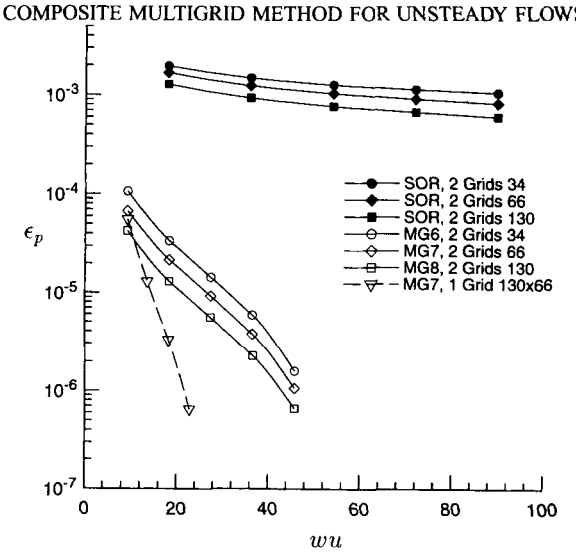

Figure 11. Residual of the pressure equation for the polar cavity flow at the first time step: ε_p, residual of the pressure equation; *wu*, working unit. Legends: for example, 2 Grids 66 denotes two component grids each consisting of a total of 66 × 66 grid points including the fictitious points

more stringent measure of solution consistency. We can see that the vorticity contours are connected smoothly through inter-grid boundaries (Figure 10(a)).

The flow whose domain is decomposed into two subgrids is used to investigate several important properties of the composite grid method. The efficiency of CMG in solving the pressure Poisson equation is demonstrated in Figure 11, in which the typical convergence behaviour is shown. The multigrid scheme with n levels is denoted as 'MGn' in the legend and ε_p is the residual of the pressure Poisson equation. An optimized overrelaxation value of 1·7 was used in the point SOR iteration. The convergence of the multigrid on a single grid is also shown for comparison. One working unit is defined as one SOR iteration on the finest grid level. We see that CMG is much superior to SOR in

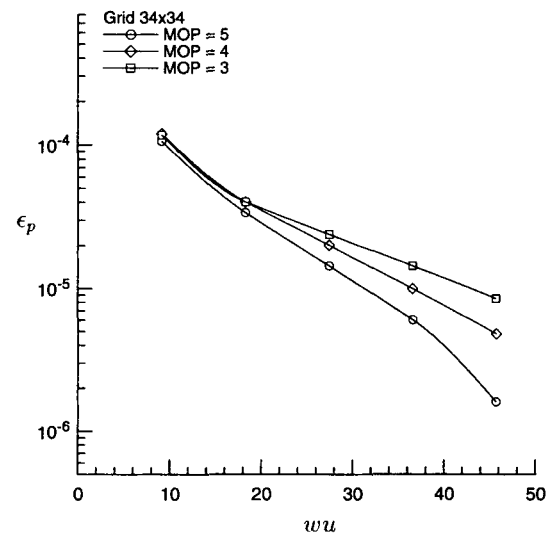

Figure 12. Effect of grid overlapping on multigrid convergence. MOP denotes the minimum number of overlapping grid points

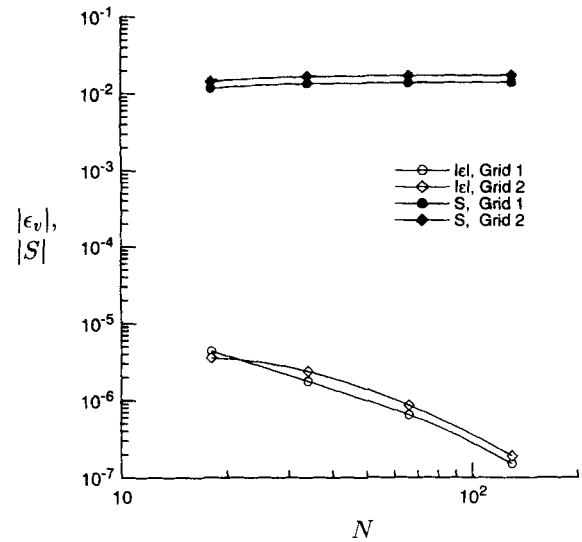

Figure 13. Absolute value of the dimensionless global mass imbalance ε and sum of the absolute values of the volume flux S as functions of mesh refinement

terms of convergence rate. Neither CMG nor SOR is very sensitive to the size of the grid. The convergence of CMG is exponential and only about twice slower than MG-CS on a single grid. We note that the convergence behaviour in Figure 11 was obtained on non-orthogonal and highly stretched grids, which demonstrates the efficiency and robustness of the present method.

The effect of the extent of grid overlapping on the convergence of CMG is also investigated. The convergence of three cases, which have corresponding minimum-overlapping points (MOPs) of 3, 4 and 5, is shown in Figure 12. The convergence is faster as the grid overlapping increases. This is consistent with the findings of Oliger *et al.*[29] and is thought to be a property of the global iteration through subgrids.

The behaviour of the MIC scheme is investigated by plotting ε_v and S in equations (24) and (25) respectively, non-dimensionalized by the appropriate length and time scales, as a function of mesh refinement (Figure 13). In all cases the flow was integrated to 1 s from start-up and *CFL* was kept fixed. We see that the value of S is essentially independent of grid size while ε_v decreases with grid size, following a slope of approximately -2. This shows that the ratio ε_v/S, and thus the correction made to $U_m^{n+1,p}$ in equation (23), is of second order, which again confirms that the MIC scheme does not degrade the second-order accuracy of the overall method.

5.3. Upwelling flow in a rotating axisymmetric container

Figure 14 shows the vertical geometry of the flow domain and the boundary conditions of the upwelling flow. The outer boundary of the container consists of a small vertical wall and a conical bottom. This was the geometry used in a previous experimental laboratory investigation of coastal upwelling flows.[30] The fluid and the container are initially in solid body rotation at an angular velocity Ω. At time $t = 0$ the top lid begins to rotate at $\Delta\Omega$ in the opposite direction relative to the rotating container. Because of the Coriolis effect, the fluid near the top surface is driven towards the centre of the container. A meridional circulation is then generated and the bottom fluid is upwelled to the top surface. We decompose the flow domain into two subdomains, which, in a horizontal plane, is similar to the decomposition used in Section 5.1 (Figure 4). The outer grid contains $34 \times 34 \times 34$ grid points and the inner grid consists of $14 \times 14 \times 34$ points. The grid points are clustered near solid boundaries.

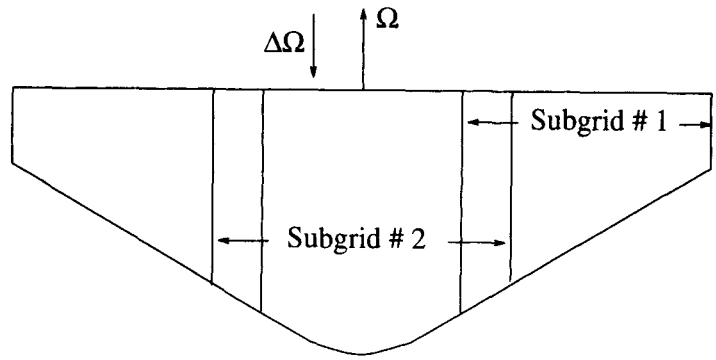

Figure 14. Schematic diagram of the domain decomposition in the vertical cross-section and the boundary conditions of the upwelling flow

The evolution of the flow is shown in Figures 15(a)–15(c), where the streamlines in a vertical cross-section through the central axis are plotted. The vertical lines in the figures are boundaries of the subdomains. The Reynolds number based on the lid velocity and the maximum radius of the container is 270. The evolution of the flow is determined by the spin-up time scale[31]

$$t_s = \frac{d}{(\nu\Omega)^{1/2}},$$

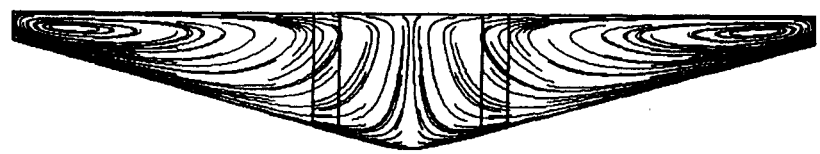

(a)

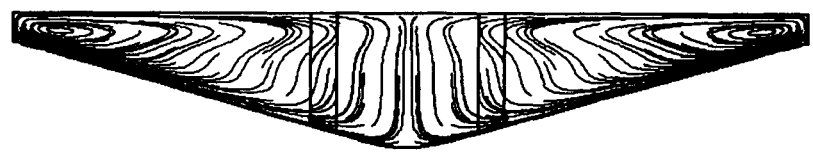

(b)

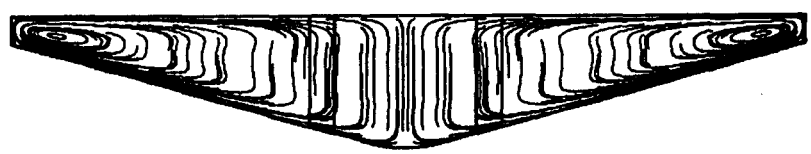

(c)

Figure 15. Streamlines in a vertical cross-section through the axis of the container: (a) $t/t_s = 0{\cdot}1$; (b) $t/t_s = 0{\cdot}3$; (c) $t/t_s = 3$

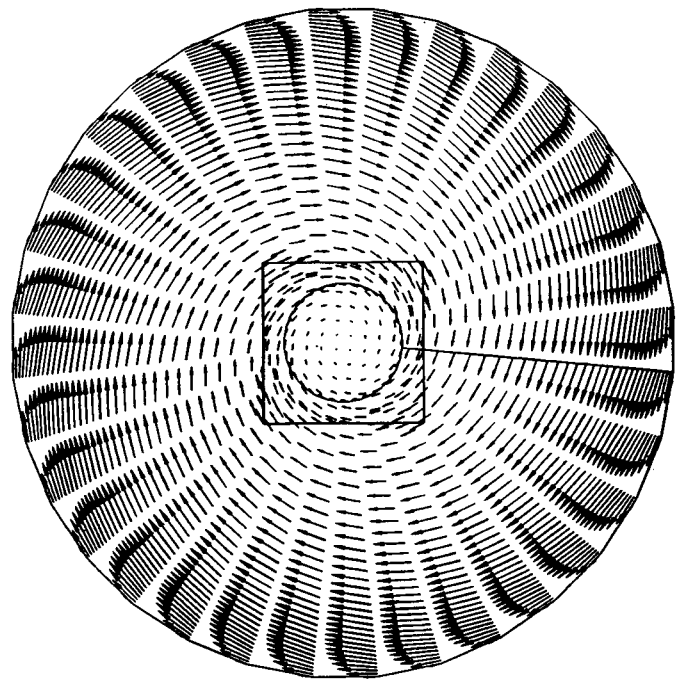

Figure 16. Velocity field in a horizontal plane near the top lid ($t/t_s = 3$)

where d is the average depth of the container, ν is the kinematic viscosity of the fluid and Ω is the angular velocity of the container.

At $t/t_s = 0{\cdot}1$ (Figure 15(a)) the Ekman layer is formed at the top lid by the Coriolis force, where fluid moves towards the central axis. Mass conservation forces the fluid to return to the outer wall in the boundary layer on the sloping bottom. At this time the interior flow is not affected by rotation and is mainly driven by the requirement of mass conservation. At $t/t_s = 0{\cdot}3$ (Figure 15(b)) rotation has begun to affect the interior flow and the streamlines are curved to adjust to the Coriolis force. At $t/t_s = 3$ (Figure 15(c)) the entire flow is dominated by rotation. In the interior the streamlines are vertical and the gradient in the vertical direction vanishes. We see that in all three cases the streamlines are connected smoothly in the overlapping zone of the subdomains, which shows the consistency of the present method on a non-orthogonal grid. Figure 16 shows the velocity vector field in the horizontal plane at the peak of the top Ekman layer at $t/t_s = 3$. The grid boundaries are also shown. Consistency of the composite grid solution is again demonstrated.

6. CONCLUSIONS

A numerical method is developed to solve the three-dimensional incompressible Navier–Stokes equations on a composite grid with arbitrary subgrid overlapping. The iterative boundary velocity scheme which is developed in the present work satisfies the condition of well-posedness and is crucial in order to achieve the consistency of solutions in arbitrarily overlapping grids. The composite multigrid (CMG) method together with the mass imbalance correction (MIC) scheme shows an excellent convergence rate when solving the pressure Poisson equation. The overall solution method is second-order in both space and time. The test results show that the composite grid solutions have an accuracy comparable with that of the single-grid solutions with similar grid size.

ACKNOWLEDGEMENTS

The authors wish to thank Professors J. R. Koseff, J. Ferziger and J. Oliger and Dr. C. Y. Perng for many helpful discussions. The research was supported by the National Science Foundation through Grant CTS-8719509. A Cray Y-MP allocation by the San Diego Supercomputer Center is gratefully acknowledged.

APPENDIX: ORDER OF ACCURACY OF THE MIC SCHEME

The global mass conservation on a subdomain is enforced by the mass imbalance correction (MIC) scheme given in equations (23)–(25). They are repeated here:

$$\bar{U}_m^{n+1,l} = U_m^{n+1,l} - \frac{\varepsilon_v |U_m^{n+1,l}|}{S} \frac{\mathbf{n} \cdot \mathbf{e}_m}{|\mathbf{n} \cdot \mathbf{e}_m|} , \tag{30}$$

where $U_m^{n+1,l}$ denotes the volume flux at the lth pressure iteration at time step $n+1$, $\bar{U}_m^{n+1,l}$ is the volume flux after the correction, ε_v is the global mass imbalance and S is the sum of the absolute values of the volume fluxes over all inter-grid boundaries;

$$\varepsilon_v = \sum_{\delta\Omega_i} \left(U_m^{n+1,l} \frac{\mathbf{n} \cdot \mathbf{e}_m}{|\mathbf{n} \cdot \mathbf{e}_m|} \right) , \tag{31}$$

$$S = \sum_{\delta\Omega_i} |U_m^{n+1,l}| , \tag{32}$$

where $\delta\Omega_i$ denotes all the inter-grid boundaries of the subdomain under consideration, $\mathbf{e}_m$ is the unit vector in the direction of the co-ordinate line ξ_m and $\mathbf{n}$ is the outward unit vector normal to the surface of the inter-grid boundary.

The Cartesian velocity components are interpolated from neighbouring subdomains to compute the volume flux. In the following we denote the exact solution with a subscript 'e'. Since the discretization is second-order-accurate and the interpolation is third-order-accurate, the interpolated Cartesian velocity is second-order-accurate, i.e.

$$u_i^{n+1,l} = (u_i^{n+1})_e + O(\Delta x^2) , \tag{33}$$

where l is the iteration number and Δx denotes the grid spacing in the physical space. The volume flux is

$$U_m = J^{-1} \frac{\partial \xi_m}{\partial x_i} u_i , \tag{34}$$

and since

$$J^{-1} \frac{\partial \xi_m}{\partial x_i} \sim O(\Delta x^2) , \tag{35}$$

we have for the volume flux

$$U_m^{n+1,l} = (U_m^{n+1})_e + \delta_U , \quad \delta_U \sim O(\Delta x^4) . \tag{36}$$

Substituting equation (36) into equation (31), we have

$$\begin{aligned}\varepsilon_v &= \sum_{\delta\Omega_i}\left(\frac{U_m^{n+1,l}\,\mathbf{n}\cdot\mathbf{e}_m}{|\mathbf{n}\cdot\mathbf{e}_m|}\right)\\ &= \sum_{\delta\Omega_i}\left(\left(U_m^{n+1}\right)_e\frac{\mathbf{n}\cdot\mathbf{e}_m}{|\mathbf{n}\cdot\mathbf{e}_m|}+\delta_U\,\frac{\mathbf{n}\cdot\mathbf{e}_m}{|\mathbf{n}\cdot\mathbf{e}_m|}\right)\\ &= \sum_{\delta\Omega_i}\delta_U\,\frac{\mathbf{n}\cdot\mathbf{e}_m}{|\mathbf{n}\cdot\mathbf{e}_m|}\ ,\end{aligned} \tag{37}$$

since the exact solution satisfies mass conservation. Because in three dimensions a sum over a surface is proportional to the square of the number of grid points in each dimension

$$\sum_{\delta\Omega_i}(1)\sim N^2\sim\frac{1}{\Delta x^2}\ , \tag{38}$$

where N is the number of grid points in each space dimension, we obtain

$$\varepsilon_v\sim O\left(\Delta x^4\cdot\frac{1}{\Delta x^2}\right)\sim O(\Delta x^2)\ . \tag{39}$$

On the other hand, the absolute value of the sume of the boundary volume fluxes is

$$S=\sum_{\delta\Omega_i}\left|U_m^{n+1,l}\right|=\sum_{\delta\Omega_i}\left|\left(U_m^{n+1}\right)_e+\delta_U\right|\sim O(1)\ . \tag{40}$$

Substituting equations (39) and (40) into equation (30), we have

$$\bar{U}_m^{n+1,l}\sim U_m^{n+1,l}-\left|U_m^{n+1,l}\right|O(\Delta x^2)\ , \tag{41}$$

so that

$$\frac{\bar{U}_m^{n+1,l}-U_m^{n+1,l}}{\left|U_m^{n+1,l}\right|}\sim O(\Delta x^2)\ . \tag{42}$$

The above equation shows that the MIC scheme is second-order-accurate.

REFERENCES

1. J. A. Benek, J. L. Steger and F. C. Dougherby, 'A flexible grid embedding technique with application to the Euler equations', *AIAA Paper 83–1944*, 1983.
2. M. M. Rai, 'A relaxation approach to patched-grid calculations with the Euler equations', *J. Comput. Phys.*, **66**, 99–131 (1986).
3. R. L. Meakin and R. L. Street, 'Stimulation of environmental flow problems in geometrically complex domains, part 2: A domain-splitting method', *Comput. Methods Appl. Mech. Eng.*, **68**, 311–331 (1988).
4. R. F. van der Wijngaart, 'Composite-grid techniques and adaptive mesh refinement in computational fluid dynamics', *Ph.D. Thesis*, Department of Mechanical Engineering, Stanford University, 1989.
5. K. Stüben and U. Trottenberg, 'Multigrid methods, fundamental algorithms, model problems analyses and applications', *Lecture Notes in Mathematics*, Vol. 960, *Multigrid Methods*, Springer, Berlin, 1982, pp.
6. W. D. Henshaw and G. Chesshire, 'Multigrid on composite meshes', *SIAM J. Sci. Stat. Comput.*, **8**, 914–923 (1987).
7. M. Hinatsu and J. Ferziger, 'Numerical computation of unsteady incompressible flow in complex geometry using a composite multigrid technique', *Int. j. numer. methods fluids*, **13**, 971–997 (1991).
8. J. Y. Tu and L. Fuchs, 'Overlapping grids and multigrid methods for three-dimensional unsteady flow calculations in IC engines', *Int. j. numer. methods fluids*, **15**, 693–714 (1992).
9. M. Berger and J. Oliger, 'Adaptive mesh refinement for hyperbolic partial differential equations', *J. Comput. Phys.*, **53**, 484–512 (1984).

10. S. C. Caruso, J. H. Ferziger and J. Oliger, 'Adaptive grid techniques for elliptic fluid-flow problems', *Res. Rep.*, Center for Large Scale Scientific Computations, Stanford University, 1985.
11. S. McCormick and J. Thomas, 'The fast adaptive composite grid (FAC) method for elliptic equations', *Math. Comput.*, **46**, 439–456 (1986).
12. C. Y. Perng and R. L. Street, 'A coupled multigrid–domain-splitting technique for simulating incompressible flows in geometrically complex domains', *Int. j. numer. methods fluids*, **13**, 269–286 (1991).
13. R. G. Hindman, 'Generalized coordinate forms of governing fluid equations and associated geometrically induced errors', *AIAA J.*, **20**, 1359–1367 (1982).
14. Y. Zang, R. L. Street and J. R. Koseff, 'A non-staggered grid, fractional step method for time-dependent incompressible Navier–Stokes equations in general curvilinear coordinate systems', *J. Comput. Phys.*, **114**, 1, 18–33 (1994).
15. J. Kim and P. Moin, 'Application of a fractional-step method to incompressible Navier–Stokes equations', *J. Comput. Phys.*, **59**, 308–323 (1985).
16. B. P. Leonard, 'A stable and accurate convective modeling procedure based on quadratic upstream interpolation', *Comput. Methods in Appl. Mech. Eng.*, **19**, 59–98 (1979).
17. R. M. Beam and R. F. Warming, 'An implicit finite-difference algorithm for hyperbolic systems in conservative-law form', *J. Comput. Phys.*, **22**, 87–110 (1976).
18. W. R. Briley and H. McDonald, 'Solution of the multidimensional compressible Navier–Stokes equations by a generalized implicit method', *J. Comput. Phys.*, **24**, 372–397 (1977).
19. P. M. Gresho and R. L. Sani, 'On pressure boundary conditions for the incompressible Navier–Stokes equations', *Int. j. numer. methods fluids*, **7**, 1111–1145 (1987).
20. R. L. LeVeque and J. Oliger, 'Numerical analysis project', *Manuscript NA-81-16*, Computer Science Department, Stanford University, 1981.
21. R. L. Meakin, 'Application of boundary conforming coordinate and domain decomposition principles to environmental flows', *Ph.D. Thesis*, Department of Civil Engineering, Stanford University, 1986.
22. W. D. Henshaw, 'Part I: The numerical solution of hyperbolic systems of conservation laws. Part II: Composite overlapping grid techniques', *Ph.D. Dissertation*, California Institute of Technology, Pasadena, CA, 1985.
24. C. Y. Perng and R. L. Street, '3-D unsteady flow simulation: alternative strategies for a volume-averaged calculation', *Int. j. numer. methods fluids*, **9**, 341–362 (1989).
25. A. Brandt, 'Multi-level adaptive solutions to boundary-value problems', *Math. Comput.*, **31**, 333–390 (1977).
26. M. Rosenfeld, D. Kwak and M. Vinokur, 'A fractional step solution method for the unsteady incompressible Navier–Stokes equations in general coordinate systems', *J. Comput. Phys.*, **94**, 102–137 (1991).
27. D. J. Acheson, *Elementary Fluid Dynamics*, Clarendon, Oxford, 1990.
28. L. Fuchs and N. Tillmark, 'Numerical and experimental study of driven flow in a polar cavity', *Int. j. numer. methods fluids*, **5**, 311–329 (1985).
29. J. Oliger, W. C. Skamarock and W. P. Tang. 'Schwarz alternating method and its SOR accelerations', *Tech. Rep. CLaSSic-86-12*, Computer Science Department, Stanford University, 1986.
30. S. Narimousa and T. Maxworthy, 'Coastal upwelling on a sloping bottom: the formation of plumes, jets and pinched-off cyclones', *J. Fluid Mech.*, **176**, 169–190.
31. E. R. Benton and A. Clark Jr., 'Spin-up', *Ann. Rev. Fluid Mech.*, **6**, 257–280 (1974).